Numerical Simulation of the Convective Instability in a Dump Combustor

Habib N. Najm* and Ahmed F. Ghoniem†
Massachusetts Institute of Technology, Cambridge, Massachusetts 02139

The mechanism of the convective instability in a channel with a sudden expansion, known in combustion literature as a dump, followed by a sudden contraction is investigated. The problem is analyzed using vortex simulations at a high Reynolds number. Of particular interest is the effect of the length of the cavity between the expansion and contraction sections on the flow structure and dynamics. We show that two instabilities may be encountered, depending on the ratio of the cavity length to its depth. For short cavities, the roll-up of the separating shear layer is the dominant mode of oscillation, producing small eddies that propagate along the top of the cavity. As the length-to-depth ratio increases, a lower frequency mode is observed to coexist with the separating shear-layer mode. For long cavities, the recirculation zone behind the step sheds large-scale, low-frequency eddies that dominate the dynamics, mixing, and oscillations within the cavity.

I. Introduction and Background

THE mechanism of the convective instability of a flow over a rectangular cavity at a high Reynolds number is investigated in this paper. Experimentally, it has been observed that this flow is dominated by vortical structures that form upstream near the separation edge and impinge on the bottom wall or at the downstream edge of the cavity. The formation of these eddies is associated with large-amplitude variations of pressure and velocity. The term convective refers to the instability governed by the convective, rather than the acoustic, time scales of the flow.

Cavity flows arise in many engineering applications. We are interested in the dynamics of cavity flows when coupled with heat release due to combustion. This is relevant to premixed dump combustors in which the flame is stabilized by the recirculation of hot products downstream of a sudden expansion. The roll-up of the shear layer into large-scale eddies is essential for the stable operation of the combustor since they promote mixing. Schlieren photographs of the reacting field show that the flame front is modulated by what appears to be large-scale structures.[1] The dynamics of these structures depend on the flow and mixture conditions.[2] At high heat-release rates, flow instabilities may trigger processes that lead to flame flashback into the premixing chamber, followed by large amplitude sustained oscillations in the flame location and pressure. Experimental studies suggest that the mechanism of flashback involves an interaction between the large-scale structures behind the dump, the expansion of hot products of combustion, and the acoustic field of the system.[3,4] These observations show a strong correlation between the nonreacting flow dynamics and those of the reacting flow.[5] In this work, we investigate the nonreacting flow dynamics.

It is evident that the formation of large-scale structures is responsible for the large oscillations measured in cavity flows. However, the mechanism of formation of these eddies has not been fully understood. It has been argued that cavity flow instability is a result of an interaction between the shear-layer Kelvin-Helmholtz instability and the channel flow Tollmien-Schlichting (TS) waves.[6] Another view holds that it is the acoustic modes of the system that determine the roll-up frequency of a confined, separated shear layer.[7,8] However, cavity flow oscillations have been observed in incompressible flow, and when the upstream flow was free of significant TS oscillations,[9,10] suggesting the presence of different mechanisms.

Kelvin-Helmholtz instability leads to the formation of large-scale structures in free shear layers at a wide range of frequencies. The mode observed most frequently corresponds to the most unstable frequency f_n, whose Strouhal number is $St_n = f_n \theta_0/U_s = 0.033$, where θ_0 is the momentum thickness of the undisturbed layer and U_s the mean velocity in the layer.[11] The behavior of a shear layer forced by controlled external excitation has been analyzed.[12,13] Results show that the shedding frequency is the harmonic of the forcing frequency closest to the most unstable frequency. As the forcing frequency f_f is decreased, the roll-up, or the response frequency, f_r experiences jumps that correspond to the harmonics of the forcing frequency, nf_f, where n is an integer.

A shear layer impinging on a downstream wedge is exposed to forcing, due to the upstream influence of the disturbance generated by the impingement of flow structures on the downstream wedge.[14,15] An impinging shear layer was found to exhibit jumps in its oscillation frequency with the variation of impingement length L, mainstream velocity U_0, and separating boundary-layer momentum thickness θ_0. These jumps correspond to changes in the number of eddies that exist simultaneously within L. In all cases, the eddy impingement frequency f_i, the same as the feedback frequency from the downstream edge f_f, is equal to the roll-up frequency.

Pressure fluctuation frequencies at the downstream impingement point of a rectangular cavity in a channel are found to scale with L and U_0, such that $fL/U_0 = 0.5(n + 1/4)$.[16,17] This relation is based on the assumption that $L/\lambda = n + 1/4$, and $c/U_0 = 0.5$, where λ and c are the wavelength and phase velocity of the strongest oscillation, respectively, and $\lambda = c/f$. This relation was confirmed for a relatively wide range of cavity lengths, $L/D = 0.3 - 5.5$, where D is the depth of the cavity, and at a high Reynolds number, $U_0 D/\nu = 7 - 9 \times 10^5$, where ν is the kinematic viscosity. The frequency with the highest amplitude experienced jumps between three stages corresponding to $n = 1$, 2, and 3 as the value of L/D was changed.

It was also found that $L/\lambda = n$ for a planar ramp-cavity geometry, with L/D around 2.0.[10] In this case, the frequency

Presented as Paper 87-1874 at the AIAA/SAE/ASME/ASEE 23rd Joint Propulsion Conference, June 29–July 2, 1987, San Diego, CA; received Sept. 25, 1989; revision received Feb. 7, 1990.

*Member of the Technical Staff, Texas Instruments, Dallas, TX.
†Associate Professor, Department of Mechanical Engineering. Associate Fellow AIAA.

with the highest peak experiences jumps with the variation of L/θ_0, such that $St = f\theta_0/U_0 = 0.011 - 0.018$. Oscillations in an axisymmetric cavity, with $L/D < 1.1$, were found to follow $L/\lambda = n + 1/2$.[18] The cavity depth D affects the dynamics if it is less than $5 - 10\delta_0$, where δ_0 is the boundary-layer thickness at the upstream separation edge, defined as the point where $u/U_0 = 0.99$. Recent review papers provide a detailed account of impinging and cavity flows.[19,20]

A cavity flow is complicated beyond the simple shear layer by the presence of the downstream edge, the existence of recirculating eddies inside the cavity, and the interaction of the shear layer with the cavity floor and the disturbances in the channel. According to experimental information, the frequency of oscillation depends on L, D, U_0, θ_0, and the Reynolds number Re. For a cavity in a channel, the channel height H may also be important. Although the flow structure and instability mechanism for short cavities, $L/D < 2$, have been studied in detail,[9] longer cavities, $L/D > 2$, have not received similar attention.[17] The dynamics of long cavities appear to be inherently different from that of short cavities due to the interaction between the separating shear layer and the cavity floor, and the instability of the recirculation zone and the shedding of large-scale eddies. Low-frequency oscillation has been reported, but is not well understood.

The paper is organized as follows. In Sec. II, the model problem is described and the numerical method briefly discussed. Section III follows with an analysis of the numerical results for a short and long cavity, where we elaborate on the differences between the instability mechanism in both cases. Conclusions are presented in Sec. IV.

II. Problem and Method of Solution

We investigate an incompressible flow over a rectangular cavity inside a channel. The geometry of the channel is shown in Fig. 1. The flow is assumed to be two-dimensional. This is not expected to incur major errors since the large-scale structures, which are expected to dominate the flow dynamics, have been found to be predominantly two-dimensional.[21,22] However, this assumption should be taken with caution since the interaction of the shear layer with boundary layers tends to result in a faster transition to three dimensionality than that observed in free shear layers. The velocity profile at the inlet can be specified as desired. The flow is at a high Reynolds number, $Re_D = U_m D/\nu > 1000$, where cavity oscillation has been observed. The mean streamwise velocity in the channel is U_m.

The governing equations are the Navier-Stokes equations. Numerical solutions for the cavity flow are obtained using the vortex method. This is a direct simulation scheme that does not require turbulence modeling at a high Reynolds number. The vorticity field is calculated without averaging the governing equations and detailed information about the instantaneous flowfield is obtained. The method is Lagrangian and the computations are concentrated around areas of nonzero vorticity. Thus, it is optimized for maximum spatial resolution. The computations are grid-free, allowing for a complicated geometry to be treated with flexibility. The method is particularly useful at high Reynolds numbers when the effect of molecular diffusion is small and is confined to the wall regions and around corners.

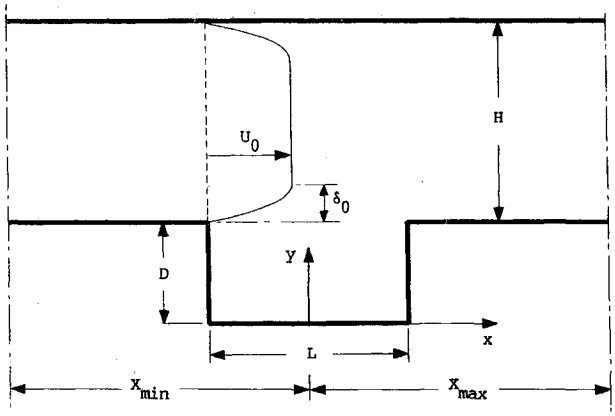

Fig. 1 Schematic diagram of the geometry of the cavity in a channel, showing the coordinate system and the parameters used to define the flow and dimensions of the computational window.

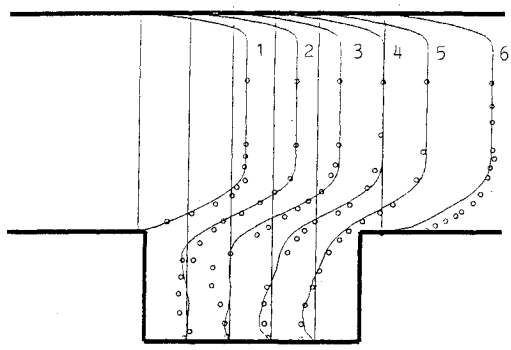

Fig. 2. Comparison between the computed mean velocity profiles (solid lines), and the measurements of Sinha,[30] (open circles), for a flow at $Re = U_0 D/\nu = 2140$, $L/D = 2$.

Recent numerical studies have established the accuracy of the vortex method by comparing the computed results with experimental data on shear layers and recirculating flows at intermediate and high Reynolds numbers.[23,24] The formulation used here utilizes vortex elements with a sharp cut-off.[25,26] This core was used in all our previous computational tests on the accuracy and convergence of the method. Vortex elements are generated as vortex sheets along the walls to satisfy the no-slip condition and transformed into vortex disks as they diffuse into the interior of the field. Vortex elements produce a rotational velocity component that is obtained form the Biot-Savart law. Their motion, according to the vorticity transport equation, is decomposed into two parts: a convective part computed by regarding the vortex elements as material points, and a diffusive part simulated by a carefully selected random walk process.[27]

The potential boundary condition along the boundaries is satisfied by adding an irrotational velocity field that is constructed to eliminate the normal velocity induced by the vorticity field along the boundaries. This is accomplished by computing the image system of the vortices using numerical conformal transformation.[28] In Ref. 29, it was shown that the numerical parameters that control the accuracy of the vortex method are the circulation per vortex element Γ, the vortex sheet length h, the sheet layer thickness Δ_s, and the time step Δt. In our computations, we refined these parameters until we established numerical convergence. The values used will be stated in the results section.

III. Results and Discussion

Results of vortex simulation of cavity flow are now analyzed. We concentrate on values of L/θ and Re where flow oscillation has been observed. The purpose of our analysis is to define the mechanism of oscillation at different values of L/D and L/θ and determine the frequency in each case.

The following discussion deals with the dynamics of short and long cavities separately. It is difficult to define a value for L/D at which one can distinguish between a short and long cavity. We make the distinction on the basis of the dynamics of the separating shear layer. If the shear layer impinges on the downstream edge before it reaches the bottom wall, we call this a short cavity. If the shear layer impinges on the bottom wall first, even though this may happen intermittently, this is a long cavity. We found that $L/D > 2$ corresponds to a long cavity. The case with $L/D = 4$ is more interesting for dump combustor analysis. However, we start with $L/D = 2$ because it represents a natural extension for the impinging shear layer.

A. Short Cavity

In this case, $L/D \leq 2$, and the separating shear layer impinges on the downstream edge before it reaches the bottom wall. In the following, we compare the computed mean velocity with experimental measurements and study the dynamics of the shear layer in terms of the roll-up of vortex eddies.

1. Mean Velocity Profiles

Figure 2 shows a comparison between the numerical results and the measurements of Sinha.[30] The parameters used in his wind-tunnel experiment are $L/D=2.0$, $\delta_0/D=0.56$, and $U_0D/\nu=2140$. The numerical parameters in our simulation are $h/D=0.25$, $\Gamma/U_mD=0.0208$, $\Delta tU_m/D=0.1$, and $\Delta_s/D=0.0207$. Vortex elements were deleted at $X_{max}/D=4$. The experimental value of the boundary-layer thickness at the step was obtained numerically by varying the inlet channel length and the velocity profile at X_{min}. The computations were performed until a stationary state was reached, and a sample of 1050 time steps was collected to obtain velocity averages.

Figure 2 shows good agreement between the computed profiles and experimental results. Two places where disagreement is noticable are the lower parts of profiles 2 and 3. Within this region, the accuracy of the experimental profiles is less certain, as confirmed by the author and evident in profile 2 where two velocity values were reported at the same location. The disagreement in the boundary-layer region of profile 6 is probably due to both three-dimensional effects and the fact that vorticity is deleted at $X_{max}/D=4.0$ for computational efficiency.

The comparison between the computed mean velocity profiles with those measured by Rockwell and Knisely[9] is shown in Fig. 3. In the experiment, $\theta_0/D=0.014$, $L/D=2$, $U_0D/\nu=7571$ (water). The numerical parameters are $h/D=0.25$, $\Gamma/U_mD=0.0208$, $\Delta tU_m/D=0.1$, $\Delta_s/D=0.015$, and $X_{max}/D=4$. Figure 3 depicts the normalized velocity u/U_{max} plotted against a normalized coordinate $(y-y_{1/2})/\theta$ at $x/D=0.92$. Here, U_{max} is the maximum velocity at the specified x location, x and y are as defined in Fig. 1, $y_{1/2}$ is the value of y at which $u/U_{max}=0.5$, and θ is the shear-layer momentum thickness at the specified x location, between $u=0$ and $u=U_{max}$. No experimental data are provided in the recirculation zone.

2. Dynamics of a Short Cavity

The flow dynamics of a short rectangular cavity, $L/D=1$–2, were investigated experimentally by Rockwell and Knisely.[9] The flow displayed jitter in the location of impingement of the shear layer on the downstream cavity edge that, they suggested, could be due to low-frequency modulation by the recirculation zone inside the cavity, as well as three-dimensional effects. A peak in the frequency spectrum was identified at

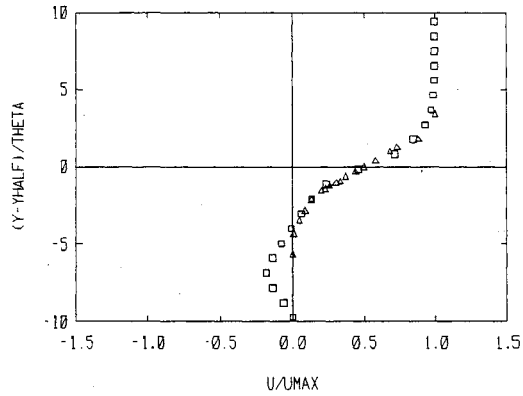

Fig. 3 Comparison between the numerical solution, (□), and Rockwell and Knisely's measurements,[9] (△), of the mean velocity profile within a cavity with $L/D=2$, and $Re=U_0D/\nu=7571$, at $x/D=0.92$.

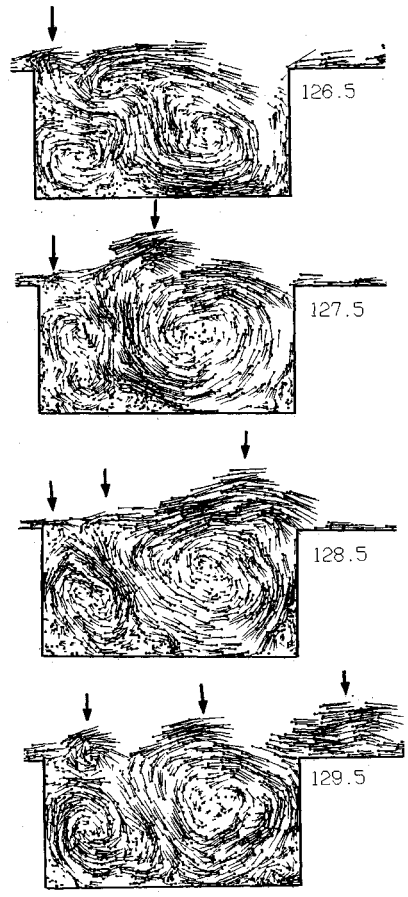

Fig. 4 Series of time frames showing the flowfield, presented in terms of the vortex elements and their velocity vectors, for the flow over a cavity with $L/D=2$ at $Re_D=7500$. The arrows indicate the centers of the separating shear-layer eddies. Note the presence of two resident eddies within the trough and the two shear-layer eddies over the impingement length.

$f\theta_0/U_0=0.016$. Knisely and Rockwell[10] studied a modified cavity, with $L/D=2$, in which the upstream edge was replaced by a slanting ramp in order to reduce the noise and enhance the organization of the roll-up process. They found that two stages of oscillation, depending on L/θ_0, may occur. In both stages, the frequency spectrum exhibited the largest peak at the shear-layer roll-up frequency, $St=0.011$–0.018 depending on L/θ_0, along with smaller peaks at lower frequencies.

The first stage corresponds to a flow structure that we refer to as a one-eddy system. In this regime, a single eddy occupied most of the impingement length, with a smaller eddy being shed from the upstream edge. The flow structure in the second stage is referred to as a two-eddy system. Here, two eddies existed simultaneously within the impingement length. In Refs. 9 and 10, the separating shear layer impinged on the downstream edge, and δ_0/D was small enough, 0.1–0.2, to minimize the interaction between the shear-layer eddies and the cavity floor. The modulation of the shear-layer dynamics by the recirculating eddies inside the cavity was observed in both stages in the form of low-frequency, global flapping of the layer.

In the numerical simulations of the short cavity, the relevant numerical parameters are $h/D=0.20$, $\Gamma/U_mD=0.0167$, $\Delta t U_m/D=0.05$, $\Delta_s/D=0.011$, and $X_{max}/D=4.0$. These parameters are more refined than those used to obtain the mean velocity distribution since here we are interested in the time-dependent structure of the flow. The flow parameters are $U_0/U_m=1.026$, $U_mD/\nu=7500$, and $\theta_0/D=0.02$. In a typical run, the number of vortex elements starts at zero at $t=0$ and grows to a value that oscillates as large eddies are shed at the step and then deleted for $x>X_{max}$. On the average, the interior

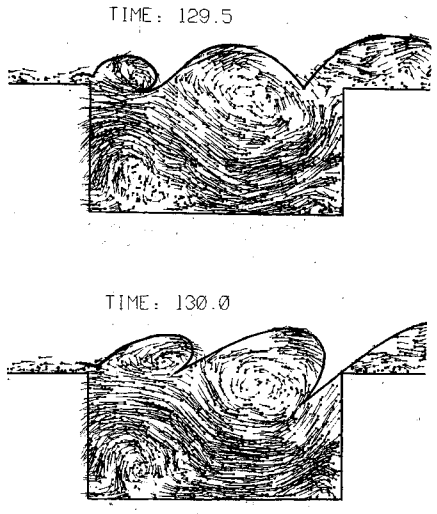

Fig. 5 Two time frames of flow depicted in Fig. 5, with the vortex elements' velocity measured with respect to $U_m/2$. A solid line, which is drawn as a demarcation of the separating shear layer, outlines a two-wave (eddy) system over the cavity.

was saturated with roughly 2200 vortex blobs, whereas the boundary layers had a total of almost 400 vortex sheets. Figure 4 shows a sequence of time frame depicting the evolution of the flow structure in terms of the vortex elements in the interior of the domain, with a straight line originating at the center of each element proportional to and in the direction of its velocity. Within this period, four eddies, marked by short arrows, are shed from the separating shear layer. The mean period between two sheddings is $T=1.17$, corresponding to $St=f\theta_0/U_0=0.0166$.

Within $t=27.0$, a total of 15 edddies were shed. These eddies can be classified in two groups, depending on their frequency, size, speed of propagation, and overall influence on the flowfield. The shedding shown in Fig. 4 represents the smaller, faster, more frequent eddies that travel in the shear layer along the top of the cavity with little effect on the recirculating flow within it. Ten such eddies were observed, nine had $St=0.013$–0.019, with a distribution skewed toward higher frequencies. One eddy had $St=0.04$. This range of $St=0.013$–0.019, where most of the shear-layer eddy-shedding occurred, is in general agreement with experimental data.

In Fig. 4, the centers of the separating shear-layer eddies are marked with an arrow. In Fig. 5, the edge of the shear layer is indicated by a solid line, while the velocity vectors are plotted with respect to a coordinate system moving at $0.5U_m$. Plotting the velocity field with respect to this moving coordinate system serves to indicate the extent and structure of the shear layer in terms of vortex structures. Both figures show the presence of two eddies within the impingement length. According to the foregoing distinction between the two regimes in a short cavity, this picture suggest that the dynamics fall in a two-eddy regime. In the laboratory reference frame, two large recirculating eddies exist within the cavity, a counterclockwise eddy downstream of the backward-facing step, and clockwise eddy occupying the other side of the cavity. A smaller eddy resides in the bottom corner of the forward-facing step of the cavity. The shear-layer eddies flow over these two large recirculation eddies. The line defines the demarcation between the vorticity-laden fluid and the mainstream irrotational flow.

The roll-up of the separating shear layer is due to its instability. The white noise, which exists in the computations due to the discrete nature of the numerical method and the random noise associated with the simulation of diffusion, acts as small perturbations at a wide range of frequencies. The fact that some eddies were shed at frequencies different from the most preferred frequency, $St=0.016$, shows that, as in the case of a free shear layer, the separating shear-layer instability is broadband.

The dynamics of the larger, slower, less frequent eddies are illustrated in Fig. 6, showing the shedding of such an eddy. Within $T=27$, five slow eddies were observed, with St as low as 0.004. Comparison of the frames shown in Figs. 4 and 6 suggests fundamental differences between the mechanism of eddy-shedding in each. The eddy forming at the separation edge in Fig. 6 travels slower than the shear-layer eddies in Fig. 4 because it generally exists at a lower level within the cavity. It grows to become significantly larger than the shear-layer eddies, and its interaction with the downstream side of the cavity leads to a significant flapping of the shear layer above the cavity. Smaller shear-layer eddies, shed at the step, ride over the stronger wave. This picture is reminiscent of the experimentally observed modulation of the separated shear layer by the low-frequency oscillation of the recirculation zone within the cavity. The slow shedding is the mechanism responsible for the low-frequency oscillation of the recirculation zone and flapping of the shear layer.

The spectrum of frequencies in the aforementioned visualization can be quantified by studying the flow velocity fluctuations at specific points. Figure 7 shows the u-velocity fluctuation at one station in the shear layer above the cavity close to the downstream edge ($x/D=0.95$, $y=D=1.0$) and the corresponding frequency spectrum. The two plots indicate the existence of strong low-frequency and weak high-frequency oscillations. Experimental results for the $L/D=2$ ramp-cavity geometry,[10] while showing a similar spread in frequencies, exhibit a higher amplitude for the frequency peak corresponding

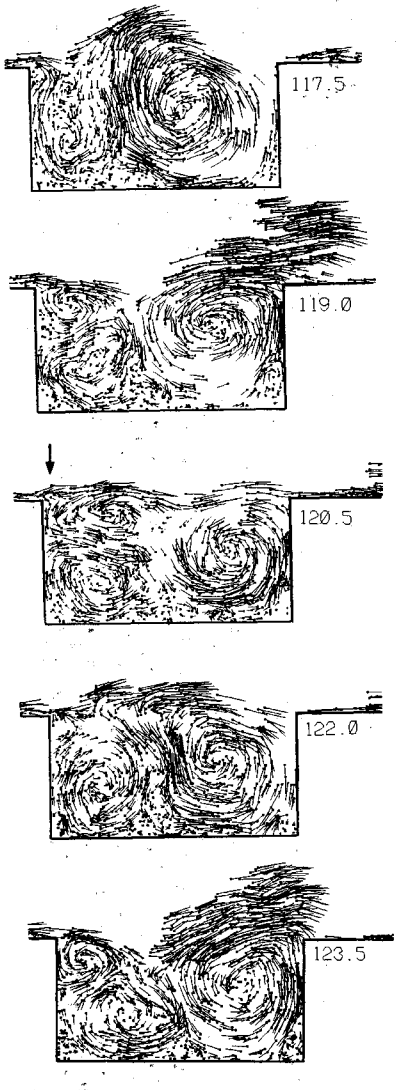

Fig. 6 Series of time frames showing the flowfield at the conditions of Fig. 4, exhibiting the shedding of a slow eddy within the cavity.

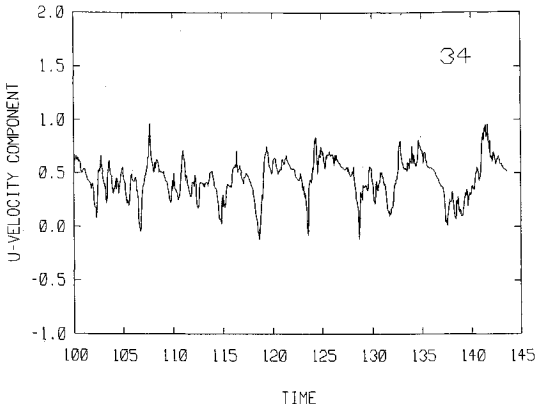

Fig. 7 Velocity fluctuation a) and frequency spectrum b) for a cavity with $L/D = 2.0$, $L/\theta_0 = 1000$ at $x/D = 0.95$, $y/D = 1.0$.

to the shear-layer eddy roll-up than for the modulation frequency. The difference between the two results indicates that the recirculation zone dynamics of the geometries considered are different. In the experimental investigation,[9] an actual cavity was used, but spectra for a shorter cavity than the one considered here were reported, namely, $L/D = 1.1$. The highest amplitude, low-frequency peak in the spectrum in Fig. 7 occurs at $St = f\theta_0/U_0 = 0.004$, or a frequency $fD/U_m = 0.22 = 1/4.5$. Thus, it corresponds roughly to the long period oscillation observed in the velocity trace in Fig. 7 and to the period of large eddy-shedding in Fig. 6.

The mean streamwise propagation velocity of the slow eddies within the cavity length is $c/U_m = 0.33$. Hence, the oscillation wavelength corresponding to the frequency $fD/U_m = 0.22$ is $\lambda/D = 1.5$. Consquently, we find $fL/c = L/\lambda = 1.33$. This result, when interpreted in terms of the formulation $L/\lambda = n$ (+ 1/2, + 1/4), suggests a value of the integer $n = 1$, indicating a first-stage oscillation, or a one-eddy system within the cavity length in the recirculation zone. This is in agreement with our definition of a one-eddy system, as demonstrated by the flow structure in Fig. 6, where the large recirculating eddy in the downstream end of the cavity occupies most its length while the smaller eddy is being shed at the upstream edge.

Flow dynamics indicate that both the shear-layer and recirculation zone modes of instability exist for the cavity geometry with $L/D = 2$. It is also evident that the shear layer does not interact directly with the bottom wall of the cavity; the recirculation eddies form a buffer between the shear layer and the cavity floor, hence, the reference to this geometry as a short cavity.

B. Long Cavity

Cavities most often used in combustion applications have $L/D \geq 4$. In this case, the dynamics are different from those of a short cavity since the separated shear layer will reach the bottom wall before impinging on the other side of the cavity. We performed several simulations for different values of L/θ_0 since it was suspected that, as in the case of a short cavity, the thickness of the boundary layer would control the dynamics within the cavity. Figure 8 shows a series of frames for the flowfield for a case with $L/D = 4$, $L/\theta_0 = 183$, $Re_D = 2500$, and $U_0/U_m = 1.04$. The numerical parameters are $h/D = 0.25$, $\Delta t\, U_m/D = 0.1$, $\Gamma/U_m D = 0.0208$, and $X_{max}/D = 4$.

The numerical results reveal that 1) the flow structure is different from that observed in the short cavity and, in particular, the large eddies that reside permanently inside the short cavity are now in constant transition; and 2) the dominant frequency of oscillation is associated with the motion of the recirculation eddy away from the step and the formation of another eddy. This motion is perfectly periodic, and all the events associated with a single period are repeated every cycle. In the following, we analyze one cycle of events using a sample of frames for $t = 70$–83.

At $t = 70$, the flow structure consists of a large leading eddy moving toward the cavity edge and a "satellite" counterclockwise eddy residing between the leading eddy and the step. There are two small eddies flowing on the top side of these two large eddies. For $t = 71$–79, a new trailing eddy, with its own satellite counterclockwise eddy, forms at the step while the leading eddy is moving into the downstream edge. The trailing eddy starts as a roll-up eddy in the separating shear layer. Instead of moving on top of the large eddies, it is anchored at the step, growing by entraining more of the vortex fluid delivered by the shear layer. The shear layer rolls up, shedding small eddies that are engulfed by the growing anchored eddy.

The interaction between the trailing eddy and the step corner results in the generation of another satellite counterclockwise eddy, shown at $t = 78$. As the trailing eddy grows by entraining more vortex fluid, its satellite counterclockwide eddy grows. The trailing eddy then moves downstream, and a gap is generated between it and the step side wall, as seen at $t = 78$–80. Within the next part of the cycle the separating shear layer at the step will shed a new eddy that will become the new trailing eddy, while the first eddy will become the leading eddy.

The leading eddy grows on the right-hand side of the trough while the trailing eddy is growing on the left-hand side. As soon as the trailing eddy separates from the step, it ceases to entrain vortical fluid from the shear layer, as shown at

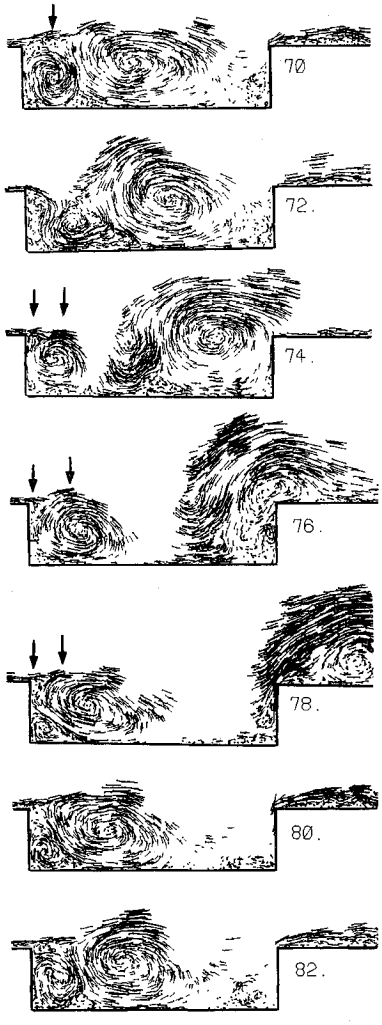

Fig. 8 Flowfield, shown in terms of the vortex elements and their instantaneous velocity vectors, for a flow over a long cavity with $L/D = 4$, $L/\theta_0 = 183$, and $Re_D = 2500$. The arrows indicate the eddies within the separating shear layer as they are shed and engulfed by the trailing, clockwise rotating eddy. Note the leading and trailing eddies, and their satellite counterclockwise rotating eddies.

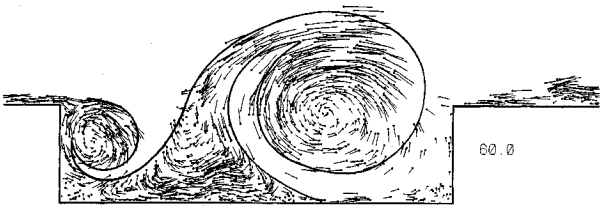

Fig. 9 Flowfield at the same conditions as in Fig. 8, with a line depicting the boundary between the vortex-laden flow and the potential flow entrained from the main stream.

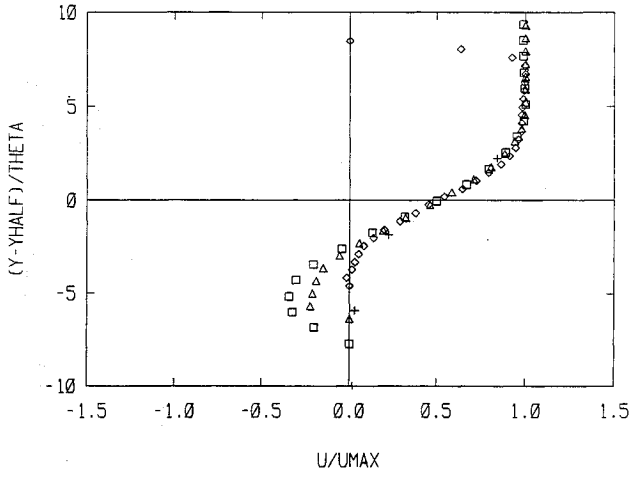

Fig. 10 Mean velocity profiles of the flow depicted in Fig. 8, exhibiting the self-similarity of the flow within the shear layer formed by the eddies shed from the recirculation zone; $x/D=-1.9$ (+), $x/D=-1.0$ (□), $x/D=0.0$ (△), $x/D=1.0$ (◇).

$t=72$–74. Instead, it becomes the leading eddy and starts to entrain nonvortical fluid from the main stream, as well as some of the vortical fluid from its satellite counter-rotating eddy. The leading eddy tends to exert a strong strain field on its satellite, causing it to become engulfed in its own field, as shown at $t=74$–78. This causes a substantial increase in the leading eddy size in the cross-stream direction. During the final stages of the leading eddy within the trough, it collides with the downstream edge of the cavity, rides over the edge, and leaves almost in its entirety, as shown at $t=76$–80.

The long cavity acts as a shallow trough in which the separating shear layer experiences large amplitude flapping on top of the recirculating eddy. This flapping causes the shear layer to interact directly with the cavity floor during part of the cycle, as opposed to the flapping observed in the short cavity where the shear layer did not interact with the floor. The recirculation zone sheds eddies that form, grow, leave the step, and are then replaced, hence causing the flapping of the shear layer. The flapping action dominates over the shedding of eddies from the separating shear layer. While these eddies are still shed at a fast rate as in the $L/D=2$ case, they do not move along the top of the cavity toward the downstream edge as in Fig. 4. Instead, they are instantly engulfed by the recirculating zone eddies. Most of the entrainment from the main stream takes place within the eddies generated in the recirculation zone, as shown in Fig. 9 in which a dark line is drawn to indicate the boundary between the vortex fluid and the irrotational fluid entrained from the main stream. The flow structure in Fig. 9 is reminiscent of the entrainment contours in free shear layers.

Average velocity profiles within the cavity are shown in Fig. 10. The profiles exhibit self-similarity within the shear layer, $0<u<U_{\max}$. The growth of the recirculation eddies, shown in terms of the average momentum thickness $\theta(x)$, is depicted in Fig. 11. Figure 11 shows a plot of θ/θ_0 vs $(x-x_{eup})/\theta_0$ for five x locations along the cavity length, $x=-2$, -1.95, -1, 0, and 1, where $x_{eup}=-2$ is the x location of the upstream cavity edge. The two phases of development of the eddy, involving its being either the trailing or leading eddy, are shown in this figure. In the first phase, the trailing eddy grows by entraining vortex fluid from the separating shear layer. The trailing eddy ceases to grow as soon as it is separated from the step. In the second phase, the trailing eddy becomes the leading eddy, and it grows by entraining fluid from the main stream and engulfing its satellite counter rotating eddy.

A time trace of the streamwise velocity component is shown at coordinates $(x/D,y/D)=(-1.0,1.0)$ and $(1.95,1.0)$ in Fig. 12. It shows the organization of the recirculation eddy-shedding process at a dimensionless time period of 12.5. Figure 13 depicts the spectra for the fluctuation in the streamwise velocity at the same stations just chosen. The highest peak occurs at $St=f\theta_0/=0.0016$, an order of magnitude smaller than the shear-layer most unstable Strouhal number. Further, since $\theta_0/D=0.0218$ and $U_0/U_m=1.040$, the frequency corresponding to this peak is $fD/U_m=0.08=1/12.5$. This peak corresponds to the frequency of recirculation eddy-shedding.

The mean streamwise propagation speed for the recirculation zone eddies is $c/U_m=0.21$. This leads to $fL/c=L/\lambda=1.52$ that, as was noted for the recirculation eddy-shedding in the $L/D=2$ case, indicates a value of $n=1$, a first-stage oscillation, and a one-eddy system in the recirculation zone, which is evident in the flow structure shown in Fig. 8.

To investigate the significance of L/θ_0 on the cavity dynamics for long cavities, we repeated the foregoing numerical simulation with $L/\theta_0=119$ and 217. Figure 14 shows velocity traces and fluctuation spectra for the two cases. The corresponding frequencies of oscillation of the recircualtion zone are the same as in the results for the intermediate case, $L/\theta_0=183$, to within the frequency resolution ± 0.007. The peak Strouhal numbers are different because θ_0 is different among the three cases. It is also noted that the extent of the time axis is different in Figs. 13, 14a, and 14b. The flowfields in all cases look like that in Fig. 8. A sample of 130 time steps is shown in Fig. 15 for $L/\theta_0=217$. These results indicate that the value of θ_0 is irrelevant to the dynamics of the flowfield in the long cavity case, as is suggested by the dominance of the recirculating zone instability over the shear-layer instability.

To study the transition between the short and long cavity, we investigated the case of $L/D=3$. In this case, the flow parameters are $L/\theta_0=123$, $Re_D=2500$, and $U_0/U_m=1.06$. The numerical parameters used are $h/D=0.25$, $\Delta t\ U_m/D=0.1$, $\Gamma/U_mD=0.0208$, and $X_{\max}=4$. The dynamics of the flowfield are shown in Fig. 16. The highest peak in the frequency spectrum, which corresponds to the recirculation zone oscillation, is $fD/U_m=0.09=1/11.1$. The phase speed, $c/U_m=0.16$, indicates that $fL/c=L/\lambda=1.69$ a one-eddy system in the recirculation zone.

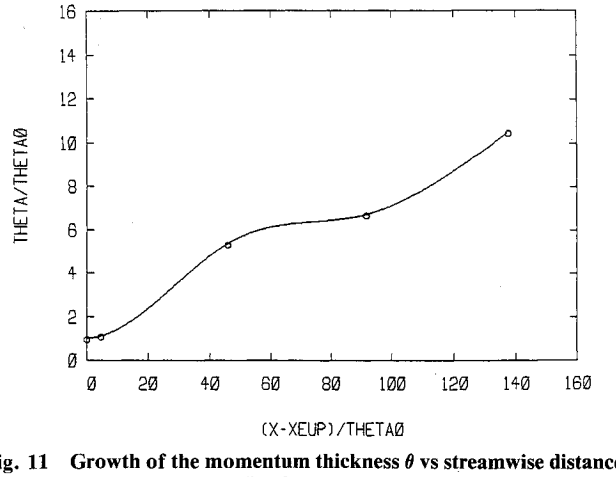

Fig. 11 Growth of the momentum thickness θ vs streamwise distance for the flowfield shown in Fig. 8.

The sequence of frames shown in Fig. 16 illustrates dynamics common to the two cases, $L/D=2$ and 4. In the time period 70–75, the trailing eddy moves downstream while growing as it entrains both nonvortical fluid and shear-layer eddies, indicated by arrows. The development of the flow starting at $t=75$ in Fig. 16 is similar to that observed in Fig. 8 starting at $t=70$. The effect of the shorter cavity length in the $L/D=3$ case is to change the development of the leading eddy. In Fig. 8, this eddy grows to the point where its center is at the level of the channel floor, before it collides with the downstream

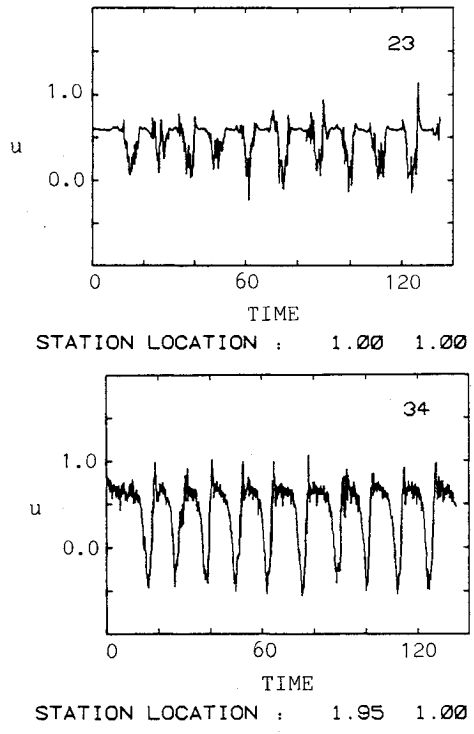

Fig. 12 Time traces of the streamwise velocity at points along the top of the cavity, for the flowfield of Fig. 8, showing the oscillation produced by the shedding of eddies from the recirculation zone. The numbers underneath each figure indicate the x and y coordinates, respectively.

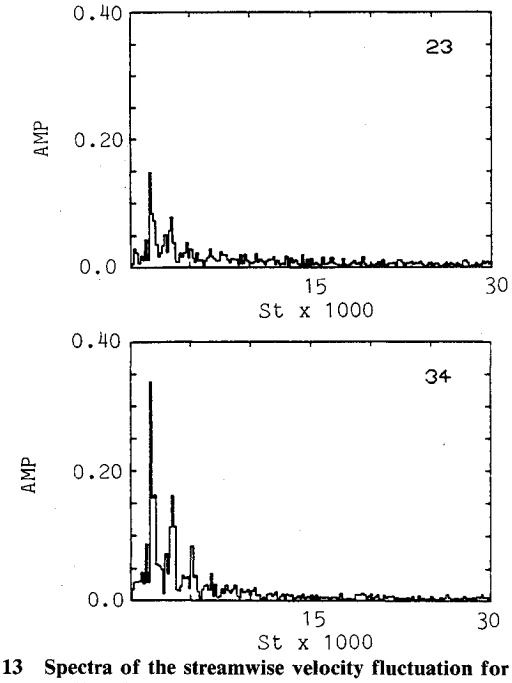

Fig. 13 Spectra of the streamwise velocity fluctuation for the same points as in Fig. 12, plotted against the Strouhal number based on the boundary-layer momentum thickness and mainstream velocity at the step.

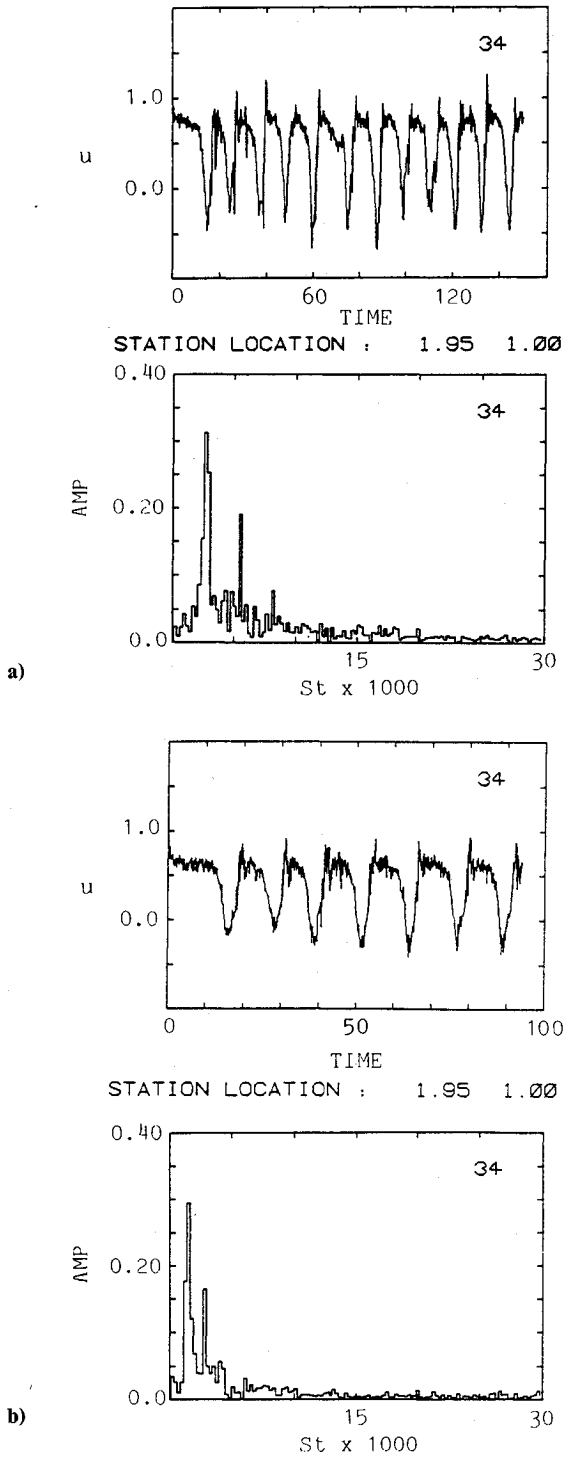

Fig. 14 Time trace and spectra of the streamwise velocity for $L/D=4$ and a) $L/\theta_0=119$ and b) $L/\theta_0=217$.

cavity step. After the collision, the eddy climbs over the step. In Fig. 16, because of the shorter distance of travel before collision, the leading eddy is smaller and its center is within the cavity when it arrives at the downstream step. In this case, the eddy is destroyed as it collides with the step. The top part of the eddy is sheared off by the faster channel flow, and the bottom part is trapped within the cavity. This process resembles the $L/D=4$ case in that all the vortical fluid comprising the leading eddy leaves the cavity as a coherent eddy, and also resembles the $L/D=2$ case in that the leading eddy is sheared off at the top by channel fluid.

It is clear from studying this intermediate case how decreasing the cavity length would decrease the amplitude of flapping of the shear layer. When L decreases, the recirculating eddies

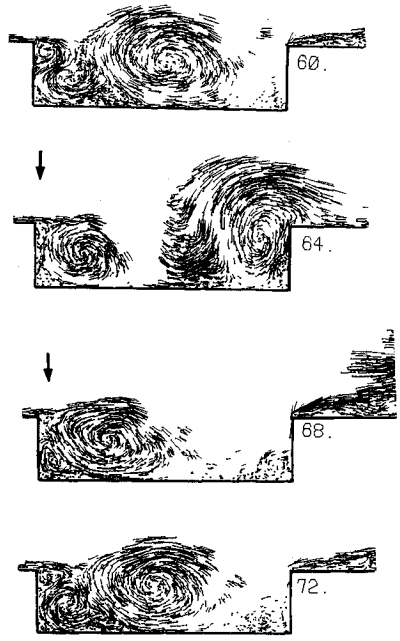

Fig. 15 Flowfield, shown in terms of the vortex elements and their instantaneous velocity vectors, over a cavity with $L/D=4$, $L=\theta_0=217$, and $Re_D=2500$. Arrows show the separating shear-layer eddies.

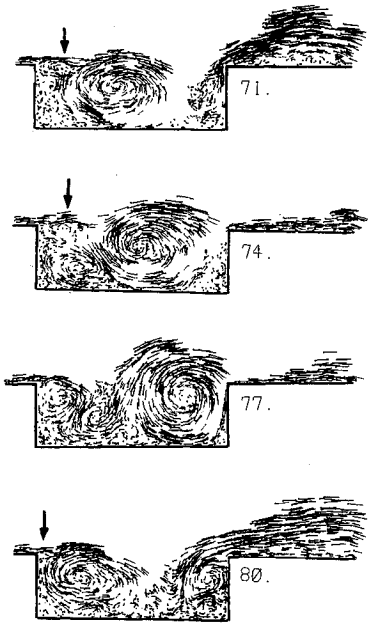

Fig. 16 Flowfield, shown in terms of the vortex elements and their instantaneous velocity vectors, over a cavity with $L/D=3$, $L/\theta_0=123$, and $Re_D=2500$. Arrows show the separating shear-layer eddies.

have less time to grow before impinging on the downstream edge and hence will grow to a smaller final size. The smaller recirculation eddy size at impingement causes smaller vertical displacement of the shear layer at that location, hence, weaker flapping. This explains the dominance of the recirculation zone instability, manifested by the flapping, over the shear-layer instability in long cavities.

IV. Conclusions

Numerical simulation of the flow over a cavity in a channel at high Reynolds number shows that the dynamics of cavity flows involve two coexisting flow instabilities: the shear-layer instability and recirculation zone instability. If the recirculation zone were quiescent, the flowfield over a cavity would resemble a shear layer impinging on a downstream wedge, with the resulting organization due to disturbance feedback from eddy impingement downstream. However, recirculation zones are not quiescent. They have been observed, experimentally and numerically, to display low-frequency oscillation in various flow configurations. Our results illustrate how this oscillation modulates the shear-layer dynamics, causing a low-frequency flapping of the shear layer. The amplitude of flapping increases with the length of the cavity, whereas the effect of the shear-layer roll-up at the separation edge, which coexists with this global flapping, becomes increasingly negligible.

Our results show that the mechanism that drives the low-frequency oscillation of the recirculation zone is the shedding and downstream migration of large-scale eddies within the cavity. The question that still remains is what causes the organization of these eddies in the cavity flow, as opposed to, for example, a step flow where they are known to exhibit a broad spectrum.[31,32] The distrubance feedback argument may not apply here because the trailing eddy is seen to exist well before the leading eddy impinges on the downstream edge. Moreover, the organization of the separating shear-layer roll-up due feedback or external forcing does not seem relevant to the dynamics of the recirculation eddies. Another feedback mechanism involves a condition of a π phase angle between the volume fluctuation inside the cavity and the shear-layer deflection at separation.[16] This last mechanism is under investigation.

Although the cause of oscillation or eddy shedding from the recirculation zone is not clear yet, it has been observed in flow visualization and numerical simulations.[29,31,33,34] In general, the frequency associated with these oscillations is smaller than that of the oscillation induced by the separating shear-layer instability. The frequency of oscillation of the recirculation zone depends on the dimensions of the cavity and the conditions of the incoming flow. Thus, a universal value for the Strouhal number cannot be easily defined. Our results and some of those cited before show that $fD/U_0=O(0.1)$.

The shedding of large-scale eddies from the recirculation zone at low frequency strongly resembles the processes observed during the unstable modes in the dump combustor.[2,3] Although heat release may affect the shedding frequency, and the rate of growth and size of the large eddies downstream, the results of the numerical simulations suggest that the mechanism of the combustor instability is strongly tied to the instability of the recirculation zone downstream of the dump. It is also conceivable that heat release, since it induces volumetric expansion within the large eddies, may augment their coherence and, thus, amplify the feedback signal.[35] This would explain why this mechanism has not been widely observed and reported for nonreacting flows, whereas it has been well documented for reacting flows.

Acknowledgments

This work was supported by the U.S. Air Force Office of Scientific Research Grant AFOSR 84-0356, the National Science Foundation Grant CBT-8709465, and the Department of Energy Grant DE-FG04-87AL44875. Computer support was provided by a grant from the John von Neumann Computer Center.

References

[1]Pitz, R.W., and Daily, J.W., "Experimental Study of Combustion in a Turbulent Free Shear Layer Formed at a Rearward Facing Step," *AIAA Journal*, Vol. 123, No. 12, p. 1937.

[2]Keller, J. O., Vaneveld, L., Korschelt, D., Hubbard, G. L., Ghoniem, A. F., Daily, J. W., and Oppenheim, A. K., "Mechanism of Instabilities in Turbulent Combustion Leading to Flashback," *AIAA Journal*, Vol. 20, No. 2, 1982, pp. 254-262.

[3]Vaneveld, L., Hom, K., and Oppenheim, A. K., "Secondary Ef-

fects in Combustion Instabilities Leading to Flashback," AIAA Paper 82-0037, 1982.

[4]Smith, D., and Zukoski, E., "Combustion Instability Sustained by Unsteady Vortex Combustion," AIAA Paper 85-1248, 1985.

[5]Ghoniem, A. F., "Effect of Large Scale Structures on Turbulent Flame Propagation," *Combustion Flame*, Vol. 64, 1986, pp. 321–336.

[6]Ghaddar, N., "Numerical Investigation of Heat Transfer Enhancement due to Oscillatory Flow over Furrowed Walls," Ph.D. Thesis, Dept. of Mechanical Engineering, Massachusetts Inst. of Technology, Cambridge, MA, 1985.

[7]Schadow, K., and Wilson, K., "Characterization of Large-Scale Structures in a Forced Ducted Flow with Dump," AIAA Paper 85-0080, 1985.

[8]Schadow, K., Wilson, K., Crump, J., Foster, J., and Gutmark, E., "Interaction Between Acoustics and Subsonic Ducted Flow with Dump," AIAA Paper 84-0530, 1984.

[9]Rockwell, D., and Knisely, C., "The Organized Nature of Flow Impingement Upon a Corner," *Journal of Fluid Mechanics,* Vol. 93, 1979, pp. 413–432.

[10]Knisely, C., and Rockwell, D., "Self-Sustained Low-Frequency Components in an Impinging Shear Layer," *Journal of Fluid Mechanics*, Vol. 116, 1982, pp. 157–186.

[11]Monkewitz, P. A., and Huerre, P., "Influence of the Velocity Ratio in the Spatial Stability of Mixing Layers," *Physics of Fluids*, Vol. 25, No. 7, 1982, pp. 1137–1143.

[12]Ho, C., and Huang, L., "Subharmonics and Vortex Merging in Mixing Layers," *Journal of Fluid Mechanics*, Vol. 119, 1982, pp. 443–473.

[13]Ghoniem, A. F., and Ng, K. K., "Numerical Study of a Forced Shear Layer," *Physics of Fluids*, Vol. 30, No. 3, 1987, pp. 706–721.

[14]Hussain, A. K., and Zamman, K. B., "The Free Shear Layer Tone Phenomenon and Probe Interference," *Journal of Fluid Mechanics*, Vol. 87, 1978, pp. 349–383.

[15]Ziada, S., and Rockwell, D., "Vortex-Leading-Edge Interaction," *Journal of Fluid Mechanics*, Vol. 118, 1982, p. 79.

[16]Rockwell, D., "Prediction of Oscillation Frequencies for Unstable Flow Past Cavities," ASME Winter Annual Meeting, New York, Paper 76-WA/FE-17, 1976.

[17]Ethembabaoglu, S., "On the Fluctuating Flow Characteristics in the Vicinity of Gate Slots," Div. of Hydraulic Engineering, Univ. of Trondheim, Norwegian Inst. of Technology, Trondheim, Norway, 1973.

[18]Sarohia, V., "Experimental Investigation of Oscillations in Flows Over Shallow Cavities," *AIAA Journal*, Vol. 15, No. 7, 1977, pp. 984–991.

[19]Rockwell, D., "Oscillations of Impinging Shear Layers," *AIAA Journal*, Vol. 21, No. 5, 1983, pp. 645–664.

[20]Rockwell, D., and Naudascher, E., "Review, Self-Sustaining Oscillations of Flow Past Cavities," *Transactions of the American Society of Mechanical Engineers*, Vol. 100, 1978, pp. 152–165.

[21]Brown, G. L., and Roshko, A., "On Density Effects and Large Structures in Turbulent Mixing Layers," *Journal of Fluid Mechanics*, Vol. 64, 1974, pp. 775–816.

[22]Oster, D., and Wygnanski, I., "The Forced Mixing Layer Between Parallel Streams," *Journal of Fluid Mechanics*, Vol. 123, 1982, pp. 91–130.

[23]Ghoniem, A. F., and Gagnon, Y., "Vortex Simulation of Laminar Recirculating Flow," *Journal of Computational Physics*, Vol. 68, 1987, pp. 346–377.

[24]Ghoniem, A. F., and Sethian, J. A., "Effect of Reynolds Number on the Structure of Recirculating Flow," *AIAA Journal*, Vol. 25, No. 1, 1987, pp. 168–171.

[25]Chorin, A. J., "Numerical Study of Slightly Viscous Flow," *Journal of Fluid Mechanics*, Vol. 57, 1973, pp. 785–796.

[26]Chorin, A. J., "Vortex Models and Boundary Layer Instability," *SIAM Journal of Sci. Stat. Comput.*, Vol. 1, No. 1, 1980, pp. 1–21.

[27]Ghoniem, A. F., and Sherman, F. S., "Grid Free Simulation of Diffusion Using Random Walk Methods," *Journal of Computational Physics*, Vol. 61, No. 1, 1985, pp. 1–37.

[28]Trefethen, L. N., "Numerical Computation of the Schwarts-Chrostoffel Transformation," Computer Science Dept., School of Humanities and Sciences, Stanford Univ., Stanford, CA, STAN-CS-79-710, 1979.

[29]Sethian, J. A., and Ghoniem, A. F., "Validation Study of Vortex Methods: Flow Over a Backward-Facing Step," *Journal of Computational Physics*, Vol. 74, No. 2, 1988, pp. 283–317.

[30]Sinha, S. N., "Two-Dimensional Laminar and Turbulent Separating Flows over Backward Facing Steps and Rectangular Cavities," Ph.D. Thesis, Indian Inst. of Tech., Kanpur, India, 1978 (available from University Microfilms International).

[31]Tani, I., Iuchi, M., and Komoda, H., "Experimental Investigation of Flow Separation Associated with a Step or a Groove," Aeronautical Research Inst., Univ. of Tokyo, Rept. 364, 1961.

[32]Eaton, J. K., and Johnston, J. P., "Low Frequency Unsteadiness of a Reattaching Turbulent Shear Layer," *Third International Symposium on Turbulent Shear Flows*, edited by L. J. Bradbury, F. Durst, B. E. Launder, F. W. Schmidt, and J. H. Whitelaw, Springer-Verlag, New York, 1981.

[33]McGuiness, M., "Flow with a Separation Bubble—Steady and Unsteady Aspects," Ph.D. Dissertation, Cambridge Univ., Cambridge, England, UK, 1978.

[34]Kailasanath, K., Gardner, J., Boris, J., and Oran, E., "Interactions Between Acoustics and Vortex Structures in a Central Dump Combustion," AIAA Paper 86-1609, 1986.

[35]Yu, K., Lee, S., Stewart, H. E., and Daily, J. W., "Vortex-Nozzle Interactions in Ramjet Combustors," AIAA Paper 87-1871, 1987.

[36]Najm, H., "Numerical Investiagation of the Instability of Premixed Dump Combustors," Ph.D. Thesis, Massachusetts Inst. of Technology, Cambridge, MA, 1989.